Explanation of NMR experiments on doped cuprates using the frustration model

Chay Goldenberg* and Amnon Aharony†
School of Physics and Astronomy, Raymond and Beverly Sackler Faculty of Exact Sciences, Tel Aviv University, Tel Aviv 69978, Israel
(Received 2 December 1996; revised manuscript received 10 March 1997)

The doping dependence of the Cu NMR line shapes measured in $YBa_2Cu_3O_{6+x}$ is explained by a planar antiferromagnetic XY model with quenched frustrated ferromagnetic bonds. A numerical algorithm for finding the ground state of the model is described, as well as a method for comparing the numerical results to the experiments. Good agreement with the experiments is obtained. [S0163-1829(97)06125-0]

I. INTRODUCTION

The important role of magnetism in the CuO_2-based superconductors has been pointed out by several authors.[1,2] For example, both $La_{2-y}Sr_yCuO_{4+x}$ and $YBa_2Cu_3O_{6+x}$ exhibit rich magnetic phase diagrams with high sensitivity to doping which indicates the important role played by disorder in determining their physical properties.[1,2]

In the insulating antiferromagnetic (AF) regime (small x,y), the doping gradually destroys the spin long-range order as seen, for example, by the decrease of the Néel temperature T_N with increased doping.[1–4] One of the effects of doping is the introduction of holes into the CuO_2 planes. At low doping, the holes are localized on the oxygen ions in these planes.[5] The influence of these holes on the magnetic behavior may be explained by the change in the sign—from AF to ferromagnetic (F)—as well as the magnitude of the exchange interaction between the Cu spins neighboring the hole. This leads to frustration which causes a canting of the spins, thus reducing the spin long-range order.[6] This canting yields a spin-mediated effective dipolar interaction between the holes, which may provide a pairing mechanism between the charge carriers in the superconducting state and explain the dependence of T_c on x in the superconducting regime.[7] Here we concentrate on the insulating AF regime.

The magnetic structure of $La_{2-y}Sr_yCuO_{4+x}$ and $YBa_2Cu_3O_{6+x}$ has been studied using various experimental techniques including nuclear magnetic resonance (NMR),[8,9] muon spin rotation (μSR),[10] and neutron scattering.[1,2] In particular, information on the dependence of the local field distribution on x can be obtained using NMR (Refs. 11,12) and μSR (Refs. 13,14) measurements. Mendels *et al.*[12] studied the AF state of $YBa_2Cu_3O_{6+x}$ for $0<x<0.3$ through Cu zero field NMR at low temperatures (1.2 and 4.2 K). They found that the line shapes could be described by a sum of Lorentzians; the peak positions and widths of the NMR lines start to change with increased oxygen doping above $x=0.15$; the dependence of the NMR Larmor frequency (peak position) and the measured half linewidth at half maximum for the central Larmor line ($\sim$90 MHz) on the oxygen doping x is shown in Figs. 1 and 2, respectively. The peak positions shift towards lower frequencies while the widths increase with increased doping. Similar qualitative results have also been reported by Matsumura *et al.*[11]

Kiefl *et al.*[14] have also studied the same material using muon spin rotation below 90 mK. They used the results of their measurements to calculate the average internal field at the muon site as well as its rms deviation. Their results are given only for a few levels of doping x. It can be seen, however, that the average field in the AF regime decreases with increased doping, whereas the rms deviation increases. Similar results for the average field in $La_{2-y}Sr_yCuO_4$ have been reported by Weidinger *et al.*[13]

In the present paper we use the frustration model[6,7] to reproduce the experimental x dependence at low temperatures by finding numerically the ground state of a two-dimensional (2D) XY AF model with a small concentration of quenched frustrated F bonds and using the results to calculate experimentally measured properties. The use of the XY model is justified by the experimental observation that the spins order in the CuO_2 planes.[15] We ignore the spin fluctuations, and take the low-temperature magnetic properties of the system to be described by its ground state.

The paper is organized as follows. In Sec. II we describe the model and the numerical procedure we have used. In Sec. III we describe the numerical results, in Sec. IV we compare them to the experimental results described above, and in Sec. V we summarize our conclusions. Details of many numerical checks of various details in our numerical algorithm can be found in Ref. 16.

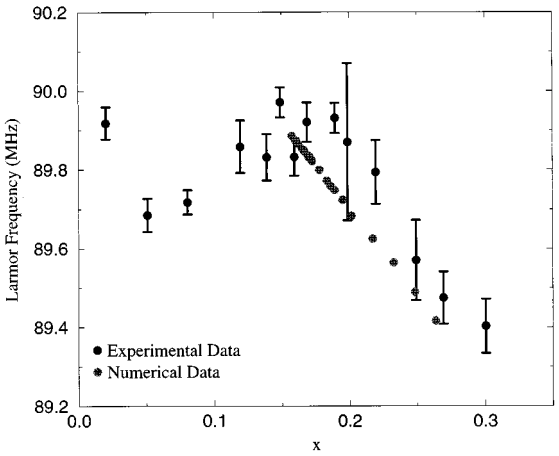

FIG. 1. The experimentally measured dependence of the NMR Larmor frequency on the oxygen content in $YBa_2Cu_3O_{6+x}$, together with our numerical results. The experimental data points were taken from Ref. 12.

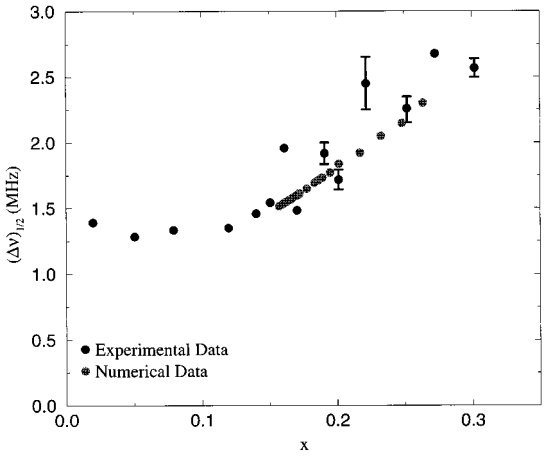

FIG. 2. The experimentally measured dependence of the measured half linewidth at half maximum for the central Larmor line ($\sim$90 MHz) on the oxygen content in $YBa_2Cu_3O_{6+x}$, together with our numerical results. The experimental data points were taken from Ref. 12.

II. THE MODEL AND THE NUMERICAL PROCEDURE

The Hamiltonian of the classical AF XY model (2D classical spins) on a square lattice is given by

$$\mathcal{H}=-\sum_{\langle i,j\rangle} J_{i,j}\mathbf{S}_i\cdot\mathbf{S}_j\,, \tag{1}$$

where $|\mathbf{S}_i|=1$. The nearest-neighbor exchange coefficient $J_{i,j}$ is AF, $J_{i,j}=-J$, for most of the bonds (we take $J=1$ for simplicity), whereas for some randomly chosen bonds we take $J_{i,j}=\lambda J$ (in our case, $\lambda=20$, see discussion below)—that is, we have an antiferromagnet with some strong F bonds.

We find it more convenient to work with a ferromagnet with some AF bonds. We therefore perform the following gauge transformation on the spins and their interactions:

$$\mathbf{S}_i=\epsilon_i\mathbf{S}_i\,,$$

$$J_{i,j}=-J_{i,j}\,, \tag{2}$$

where $\epsilon_i=(-1)^{m+n}$, m and n are Cartesian coordinates of the spins (in units of lattice constants) in the plane.

Our aim is to find the ground state of such a system. This problem is nontrivial, since the AF bonds introduce frustration; for $\lambda>1$ they cause canting of the ferromagnetically coupled spins in their vicinity: when we have a single isolated AF bond, the two spins coupled by it will align perpendicular to the average magnetization, and their neighbors will cant towards them in order to minimize the energy. Spins farther away will also cant, but to smaller extents, as we move away from the impurity (see Fig. 3). It can be shown,[6,17–20] using a continuum approximation for the spins, that far away from the AF bond the deviations of the spins from the direction of the average magnetization can be described by the Laplace equation, whose appropriate solution is a dipolar dependence on the distance and on the orientation of the spin relative to the AF bond: if the average magnetization is along the y axis, then the spin components along the x direction are given by

$$S_i^x=\boldsymbol{\mu}\cdot\mathbf{r}/r^2, \tag{3}$$

where $\boldsymbol{\mu}$ is the effective dipole moment, directed parallel to the AF bond, and $\mathbf{r}$ is the vector (in units of lattice constants) connecting the spin to the ''dipole,'' which is located on the center of the AF bond.[21]

Qualitatively, the effective dipole moment $|\boldsymbol{\mu}|$ depends on λ in the following way: for $\lambda<1$, $|\boldsymbol{\mu}|=0$. For $\lambda>1$, $|\boldsymbol{\mu}|$ increases and saturates at large values of λ. The dependence of $|\boldsymbol{\mu}|$ on λ is discussed in more detail in Ref. 16.[22] As mentioned above, we have chosen $\lambda=20$, which is in the saturation regime. Our results concerning the x dependence of the NMR line shapes do not depend significantly on λ, even for values below the saturation regime (see Ref. 16).

The dipole description introduces an additional symmetry into the problem: in addition to the usual rotation symmetry of the vector spins, there is a discrete inversion symmetry for the two spins coupled by the AF bond, which are perpendicular to the average magnetization: e.g., they can point either towards or opposite to each other. These two situations correspond to two different signs for the dipole moment $\boldsymbol{\mu}$ associated with the bond, which describes the deviations of the spins in Eq. (3). The relation between $\boldsymbol{\mu}$ and the local spin configuration around the AF bond is shown in Fig. 3.

If we have more than one AF bond, further use of the continuum approximation[6,17–19] yields the following expression for an effective spin-mediated dipolar interaction between dipoles (located on the centers of the AF bonds), namely

$$V_{ij}=-\frac{1}{r_{ij}^2}\left[\boldsymbol{\mu}_i\cdot\boldsymbol{\mu}_j-2\frac{(\boldsymbol{\mu}_i\cdot\mathbf{r}_{ij})(\boldsymbol{\mu}_j\cdot\mathbf{r}_{ij})}{r_{ij}^2}\right], \tag{4}$$

where $\boldsymbol{\mu}_i,\boldsymbol{\mu}_j$ are two dipole moments and $\mathbf{r}_{ij}$ is the vector connecting them. This expression is expected to be correct for large enough r_{ij}.[23] In our calculations we have used semi-rigid boundary conditions—that is, the spins on the lattice boundary are all kept fixed in the same direction, with a

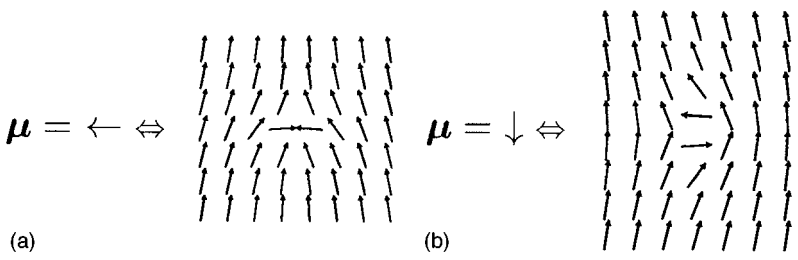

FIG. 3. The mapping between dipole orientations and local spin configurations.

weaker F coupling J' to the other spins, compared to the usual F coupling in the lattice (we used $J'=J/2$). These boundary conditions, unlike the periodic ones used in some previous papers,[19,24] enable us to use the dipole approximation as derived in the case of an infinite system, without having to consider additional contributions from periodically repeated replicas of the system using Ewald-like sums, as done by Saslow and Parker.[19] In order to use these boundary conditions we have left an outer margin of the lattice (five lattice constants wide) free of impurities, to prevent edge effects (see Ref. 16).

We now divide the problem of finding the ground state of the system into two stages: we first find the ground state of the system of dipoles; for each dipole we identify the sign of $\boldsymbol{\mu}_i$ by direct enumeration: we associate a dipole moment with each AF bond. The AF bonds are chosen randomly on the lattice by first selecting a random spin on the lattice and then selecting one of its bonds at random. We do not allow adjacent AF bonds. The dipoles are parallel to the direction of the AF bonds (see Fig. 3) and they all have the same magnitude. We then calculate the total interaction energy of the dipoles, by summing Eq. (4) over all dipoles, for each of the 2^{N-1} possible dipole configurations for N dipoles (there are two possible signs for each dipole, and we need to consider only $N-1$ dipoles since changing the signs of all dipoles will not change the energy). The ground state is then the one with the lowest dipole interaction energy.

After finding this dipole ground state, we generate the appropriate spin configuration, using the dipole approximation for the deviations of the spins from the direction of average magnetization. The contributions from each dipole to this deviation according to Eq. (3) are summed:

$$S_i^x=\sum_k \boldsymbol{\mu}_k\cdot\mathbf{r}_{ik}/r_{ik}^2, \tag{5}$$

where $\mathbf{r}_{ik}$ is the vector (in units of lattice constants) connecting the spin i to the dipole k. The two spins coupled by the AF bond are set perpendicular to the average magnetization, with signs according to the sign of the dipole in the ground state (see Fig. 3).

We assume that each dipole configuration is close to a locally stable spin configuration and that the spin ground state is close to the dipole ground state generated as described above. We therefore relax the system towards the spin ground state by iterating the local equations of motion (see, for example, Refs. 24–26):

$$\mathbf{S}_i=\frac{\mathbf{H}_i^{\mathrm{loc}}}{|\mathbf{H}_i^{\mathrm{loc}}|},$$

$$\mathbf{H}_i^{\mathrm{loc}}=\sum_{\langle i,j\rangle} J_{i,j}\mathbf{S}_j$$

(orienting each spin along its local field). The spins are updated alternately on staggered sublattices (in each half-iteration we update only spins which are not nearest neighbors), so that there is no bias in the order of spin updates. This is repeated until the criterion

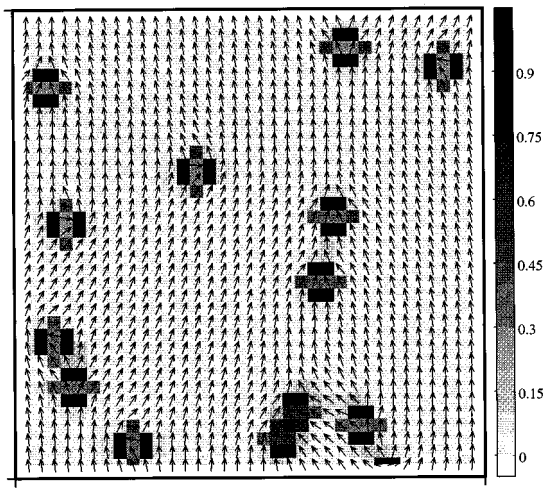

FIG. 4. A 45×45 sample spin configuration with 14 impurities, together with the values of $H'=3-H_{\mathrm{int}}$ at each spin site, where H_{int} is the effective magnetic field for NMR. The outer margin left free of impurities is not shown.

$$\sqrt{\sum_i |\mathbf{S}_{i_{\mathrm{new}}}-\mathbf{S}_{i_{\mathrm{old}}}|^2/N}\leqslant\varepsilon \tag{6}$$

is met (this is similar to the criterion used in Ref. 26). In our calculations, we used $\varepsilon=10^{-7}$.[16] We take the resulting spin configuration to be the spin ground state for the particular distribution of impurities.

As a test of the validity of Eq. (4) for more than one pair of dipoles, we relaxed (as described above) all the 2^{N-1} dipole states for several random configurations of AF bonds.[16] We found that if the distance between dipoles was kept greater than three lattice constants, the total dipole interaction energy gives a very good approximation for the total spin energy for all the dipole states and, in particular, that the lowest energy spin state among those obtained by relaxation from dipole states is found when starting the relaxation from the dipole ground state. For smaller distances between the dipoles the dipole approximation for their effective interaction [Eq. (4)] fails. Therefore, if we have dipole pairs with smaller distances, we modify the procedure in the following way. We find the dipole ground state as described above. However, we do not perform the relaxation only for the dipole ground state, but also for all the dipole states derived from it by flipping dipoles belonging to dipole pairs whose distance is smaller than four lattice constants. We then identify the spin configuration with smallest spin energy after relaxation as the global spin ground state. A sample spin configuration obtained using this method is shown in Fig. 4.

This procedure seems to be more efficient compared to the method suggested by Gawiec and Grempel[24] for treating the same problem, since in order to find the ground-state spin configuration it uses the dipole approximation for the effective interaction of the impurities for finding a spin configuration close to it, instead of using random initial configurations and then random rotations of groups of spins. It is also probably more likely to find the real ground state of the system. However, it is limited to small concentrations of

frustrated bonds—both because it relies on the dipole approximation which holds only for large enough distances between the impurities, and because we are using direct enumeration for finding the dipole ground state—which requires a computation time which is exponential in the number of impurities (this limitation may be removed by using faster methods of solving the problem, which however do not guarantee finding the exact dipole ground state).

III. NUMERICAL RESULTS

In our calculations of the NMR line shapes, we used lattice sizes from 25×25 to 85×85. The number of impurities was up to 28, leading to impurity concentrations up to $c=1.55\%$. The concentration is calculated using

$$c=\frac{N}{2(L-2W)^2}, \tag{7}$$

where N is the number of frustrated bonds, L is the lattice length, and W is the width of the outer margin kept free of impurities (see Sec. II), in units of lattice constants. In general, we found no size dependence in our results. However, in our discussion of the results we present them for all lattice sizes. In order to compare the results of our simulations to the experimental data, we need to calculate the influence of the impurity concentration on the NMR line shape. Since the NMR resonance frequency is proportional to the local magnetic field, at least part of the dependence of the NMR line shape on the hole concentration should result from changes in the distribution of the local fields acting on the Cu nuclei.

The Cu nuclear spin $\mathbf{I}_0$ is coupled not only to the electron spin of the same Cu atom but also to its four nearest neighbors, through the Hamiltonian:[27]

$$\mathcal{H}=A\mathbf{I}_0\cdot\mathbf{S}_0+B\sum_{\langle 0,k\rangle}\mathbf{I}_0\cdot\mathbf{S}_k, \tag{8}$$

where A is the component of the on-site hyperfine coupling tensor parallel to the CuO_2 plane and B is the transferred hyperfine coupling, assumed to be isotropic. $\mathbf{S}_0$ denotes the electron spin of the Cu ion and $\mathbf{S}_k$ are the electron spins of its nearest neighbors. The ratio A/B is estimated to be 0.8–1.[12,28] Taking $A/B=1$, the effective field seen by the Cu nuclear spin is proportional to

$$\mathbf{H}_{\rm int}\propto\mathbf{S}_0+\sum_{\langle 0,k\rangle}\mathbf{S}_k \tag{9}$$

(our quantitative results are not sensitive to the value of A/B in the range mentioned above).[16]

Before calculating the field distribution we perform a gauge transformation [Eq. (2)] to return to an antiferromagnet with F impurities, which is the physical case to which we compare our results. The fields at the spin sites in the outer margin left free of impurities (as mentioned in Sec. II) were not included in the calculation of the field distribution, to prevent edge effects. In calculating the field values we used Eq. (9) with the proportionality constant equal to 1, which gives $H_{\rm int}=3$ for all the sites in an undoped AF lattice (i.e., $c=0$). In order to calculate the expected NMR line shape, we need to calculate the distribution of the magnitudes of $H_{\rm int}$ over the spin lattice. Building a histogram of the values of $H_{\rm int}$ proved to be problematic, due to sensitivity to the selection of bin size (especially when trying to compare lattices of different sizes—for which we have different numbers of values of $H_{\rm int}$). Therefore we did not use the histograms for quantitative evaluations. However, it is still helpful to understand the histogram qualitatively, and a sample histogram, calculated for the lattice shown in Fig. 4 (of 45×45 spins with 14 F bonds, $c=0.0057$) is shown in Fig. 5. In the histogram we can distinguish several features: there is a large peak around $H_{\rm int}=3$. As noted above, this is the value obtained for spins which are far away from all the impurities. It is also the maximum possible value. The height of this peak decreases with increasing impurity concentration, while its width increases. Two additional, much smaller peaks can be seen around $H_{\rm int}\simeq2.15$ and $H_{\rm int}\simeq2.65$. Unlike the large peak at $H_{\rm int}=3$, their heights, as well as their widths, increase with increasing impurity concentration.

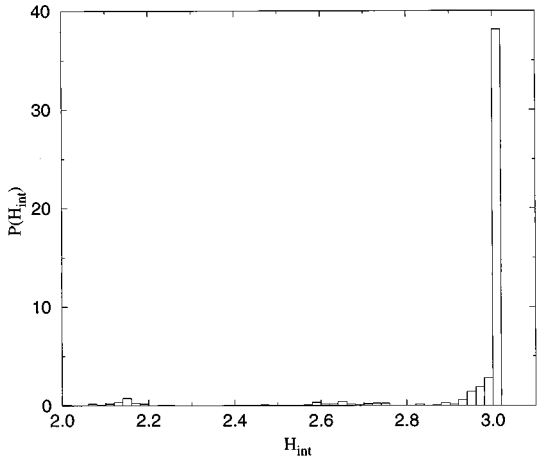

FIG. 5. A sample histogram of effective field values. The spin configuration used is the one shown in Fig. 4. A margin of five spins was ignored in the calculation of the field histogram (see text).

These features can be explained by examining the values of $H_{\rm int}$ shown for each spin site in Fig. 4. We see that different field values are obtained in different locations relative to the impurities: close to the impurities, where the relative spin orientations are very different from those in the undoped antiferromagnet, the values of $H_{\rm int}$ are very different from 3. These correspond to the small peaks observed in Fig. 5. Since each impurity contributes several sites to these peaks, their height increases with increasing impurity concentration. The peak near $H_{\rm int}=3$ is obtained from the contributions of sites which are farther away from the impurities: the field values approach $H_{\rm int}=3$ rapidly as we get farther from an impurity since in those regions the spin structure is nearly ferromagnetic. The widening of the peak with increasing impurity concentration is related to this description: as we have more impurities, we get less field values closer to 3 and more which are farther from 3.

In order to get a more quantitative explanation of the results near $H_{\rm int}=3$, we calculate the expected field distribution analytically. It is quite simple to find the field distribution for a single impurity bond. Substituting Eq. (3) in Eq.

(9) yields the following expression for the effective field magnitude $H_{\rm int}$ for each spin site:

$$H_{\rm int}(r)=3-\frac{1}{r^4}+O\left(\frac{1}{r^6}\right), \tag{10}$$

where r is the distance of the spin site from the center of the impurity bond (there is no dependence on the angle up to order $1/r^4$). We can see that the maximum value of $H_{\rm int}$ is 3, and it decreases as r decreases. We are interested in the resulting field distribution around $H_{\rm int}=3$. If we define $H'=3-H_{\rm int}$, we can then obtain $P(H')$, the distribution of H', from Eq. (10) in the following way:

$$P(H')dH'=P(r)dr=P(r)\left|\frac{dr}{dH'}\right|dH'=\frac{\pi}{2}r^6dH'$$

$$=\frac{\pi}{2}(H')^{-3/2}dH', \tag{11}$$

so that the distribution of H' has a maximum at $H'=0$ ($H_{\rm int}=3$) and it decreases as a power law (with exponent $-3/2$) at increasing H' ($H_{\rm int}$ smaller than 3). This behavior is confirmed by our numerical calculations[16] with a single impurity at the center of the lattice.

A similar calculation with more than one impurity is more complicated. We therefore estimate the peak position and width of the distribution by calculating the average field and its standard deviation, respectively. We use Eqs. (5,9) and assume there is no correlation between the dipole directions in the ground state (we neglect the correlation caused by the effective dipole interaction). We then find, for a uniform distribution of the dipoles with concentration c, that to first order in c, the average field and its standard deviation are now given by[16]

$$\langle H_{{\rm int},i}\rangle=3-\frac{3a}{2}c,$$

$$\sigma_H=\sqrt{\left(9a+\frac{9b}{4}\right)c+O(c^2)}\simeq C\sqrt{c}, \tag{12}$$

where $a\propto\Sigma_k r_{ik}^{-2}$, $b\propto\Sigma_k r_{ik}^{-4}$. The proportionality constants are of order unity. We can test this prediction by calculating these quantities numerically for different impurity concentrations (averaging over 15 samples with the same lattice size and number of frustrated bonds, but with different distributions of the frustrated bonds). We use only fields larger than 2.9 in this calculation, since we want to avoid the small peaks discussed above which are not relevant to our calculation. The numerical results are given in Fig. 6. As can be seen, the agreement with our results is quite good for concentrations up to about $c=0.008$.

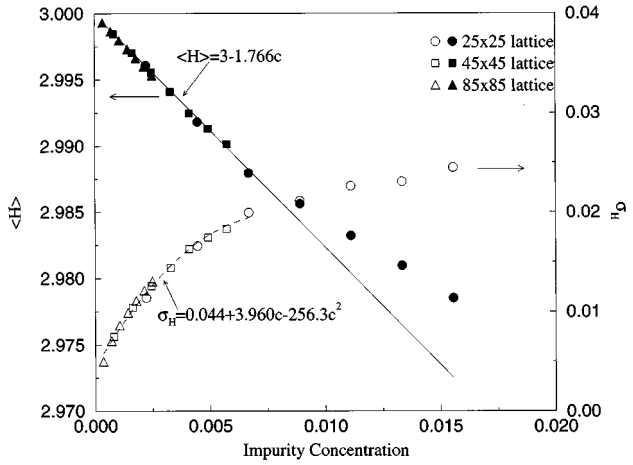

FIG. 6. The calculated average effective field (closed symbols) and its standard deviation (open symbols) as a function of the impurity concentration, for different lattice sizes, together with linear (solid line) and quadratic (dashed line) fits, respectively, performed for concentrations $c<0.008$.

IV. COMPARISON WITH EXPERIMENTS

Since experimentally there is a nonzero width of the NMR line at zero impurity concentration, in order to compare our results to the NMR experiments described in Sec. I we should take a convolution of the field distribution discussed in Sec. III with the NMR line shape at zero impurity concentration. This can be done as a direct convolution of a histogram of $H_{\rm int}$ with the Lorentzian found experimentally to describe the ''pure'' material NMR line shape, or equivalently from adding up Lorentzians centered around each local field value, with the ''pure'' NMR linewidth. We used the latter method since it avoids the problem, mentioned in Sec. III, of selecting the bin size for the histogram.

Using this method, we calculated the influence of the impurities on the NMR line shape for different impurity concentrations and for different lattice sizes. Fitting the resulting line shapes (averaged over 15 samples with the same lattice size and number of frustrated bonds, but with different distributions of the frustrated bonds) by Lorentzians (which were also used for fitting the experimental curves), we could find the dependence of properties of the line shape—namely, its peak position, its width and its intensity—on the impurity concentration (and lattice size). The line shapes were calculated with $H_{\rm int}$ on the same scale as the histograms described in Sec. III, and the relative width of the Lorentzians was chosen to be the same as the experimental one: The values of the ''pure'' experimental Lorentzian peak position and width at small oxygen concentration ($YBa_2Cu_3O_{6.08}$) were found to be 89.69 and 1.33 MHz, respectively.[12] However, these values do not seem to be representative of those presented at somewhat higher oxygen concentrations. As discussed below, we use in our calculations a ''pure'' Lorentzian width of 0.05 (the maximum field is $H_{\rm int}=3$).

In order to compare our calculations with the experimental data, we have to relate the oxygen concentration x measured experimentally to the impurity concentration c used in our model, believed to be equal to the concentration of holes n_h in the CuO_2 planes. Its relation to the oxygen doping in $YBa_2Cu_3O_{6+x}$ and $La_{2-y}Sr_yCuO_{4+x}$ or to the Sr doping in $La_{2-y}Sr_yCuO_{4+x}$ has been discussed in several experimental[29–35] as well as theoretical[36–39] papers. It is quite widely accepted that in $La_{2-y}Sr_yCuO_{4+x}$ the hole concentration in the CuO_2 planes is equal to the level of Sr or O doping.[40] In $YBa_2Cu_3O_{6+x}$ the situation is less clear: most of the existing literature concentrates on the supercon-

ducting regime, where the doping is higher than in the AF regime in which we are interested, and the different estimates are not entirely in agreement with each other. Based on the available information, we assumed that in $YBa_2Cu_3O_{6+x}$ holes are introduced into the CuO_2 planes above a certain doping level x_0, and that the dependence of the hole concentration n_h on x (in the AF regime) is linear:

$$c = n_h = \begin{cases} 0 & x \leq x_0 , \\ \dfrac{x - x_0}{\alpha} & x > x_0 , \end{cases} \tag{13}$$

where the appropriate ranges for the parameters x_0 and α are $x_0 = 0.15 - 0.2$ and $\alpha = 5 - 10$ (chosen based on the values suggested by different authors[29–39]).

A further complication is that the holes may not be localized on a single oxygen atom, so that they can affect more than one bond. The localization length at small x was actually estimated to be about two lattice constants.[41] This will probably renormalize the spin-spin exchange interactions,[18] but would not change our picture as long as λ, the ratio between the AF and F interactions, is large enough after this renormalization. We expect that at small impurity concentrations, the effective concentration of frustrated bonds will still have the behavior of Eq. (13).

Figures 1 and 2 show, respectively, our numerical results for the NMR Larmor frequency (corresponding to the peak position in our calculations) and for the linewidth of the central Larmor line (~90 MHz) together with the experimental results. The values of the peak position and width were scaled appropriately to give frequencies which can be compared with the experimental NMR results. We have found that the experimental results are fit better by our numerical ones if we take the ''pure'' Lorentzian peak position and width at zero hole concentration to be 89.9 and 1.5 MHz, respectively, implying $\sigma_{\mathcal{L}} = 0.05$. These values also seem to be more representative of the low concentration range than those given by the authors for $x = 0.08$ (89.69 and 1.33 MHz). To map our numerical results onto Figs. 1 and 2, we used $x_0 = 0.155, \alpha = 7$. These values are within the ranges given above. As can be seen in Figs. 1 and 2, the numerical results fit the experimental ones quite well.

Both the peak position and the linewidth seem to be independent of the lattice size, and to depend linearly on the impurity concentration. The linear dependence of the peak position after the convolution is consistent with our results from Sec. III. The field standard deviation found in Sec. III was proportional to the square root of the concentration. However, to calculate the width σ_{conv} after the convolution, we should add the squares of the standard deviations of the original distribution, $\sigma_H = C\sqrt{c}$, and of the Lorentzian width $\sigma_{\mathcal{L}} = 0.05$: $\sigma_{\text{conv}} = \sqrt{\sigma_{\mathcal{L}}^2 + \sigma_H^2}$. If $\sigma_H \ll \sigma_{\mathcal{L}}$ (as indeed seen from the values of σ_H in Fig. 6), we can write

$$\sigma_{\text{conv}} = \sigma_{\mathcal{L}} \sqrt{1 + \frac{\sigma_H^2}{\sigma_{\mathcal{L}}^2}} \simeq \sigma_{\mathcal{L}} \left(1 + \frac{C^2 c}{2\sigma_{\mathcal{L}}^2} \right), \tag{14}$$

so that even though σ_H is proportional to the square root of the impurity concentration, the linewidth is linear in it, as seen in our numerical results (Fig. 2).

In the experimental results, the NMR linewidth seems to deviate from its low concentration constant value at x as low as 0.12 (see Fig. 2). This is lower than the typical oxygen concentration at which most experimentally measured quantities in $YBa_2Cu_3O_{6+x}$ start to differ from their low concentration values. This experimental behavior is still consistent with our numerical results if we allow x_0 to be equal to 0.12. This would also be consistent with the dependence of the peak position on the oxygen concentration (Fig. 1). We cannot explain, however, the apparently observed minimum in the peak position found around $x = 0.05$.

V. CONCLUSIONS

We found that the dipole approximation for the spin canting and effective impurity interaction is valid even at quite small distances. The numerical procedure we describe is useful for finding the ground state of systems with low impurity concentrations.

The good agreement with the experimental results indicates that the frustration model gives a good description of the spin structure in the (low doping) doped AF regime at low temperature. The agreement with the experimental results can also be interpreted as affirming the relation we have used between hole concentration and oxygen concentration in $YBa_2Cu_3O_{6+x}$ [Eq. (13)], as well as the fact that the ratio λ between the F interaction on impurity bonds and the AF interaction on the other bonds is indeed in the saturation regime (that is, significantly larger than 1). We note that the height of the small peaks in the internal field distribution described in Sec. III increases with doping, and they may be observed experimentally in the AF regime at higher doping.

ACKNOWLEDGMENTS

We acknowledge discussions with I. Ya. Korenblit, and support from the Israel Science Foundation and from the German-Israeli Foundation for Scientific Research and Development.

*Electronic address: chayg@fractal.tau.ac.il

†Electronic address: aharony@post.tau.ac.il

[1] J. Rossat-Mignod, L. P. Regnault, P. Bourges, P. Burlet, C. Vettier, and J. Y. Henry, in *Selected Topics in Superconductivity*, edited by L. C. Gupta and M. S. Multani (World Scientific, Singapore, 1992), p. 265.

[2] G. Shirane, R. J. Birgeneau, Y. Endoh, and M. A. Kastner, Physica B **197**, 158 (1994).

[3] H. Alloul, T. Ohno, H. Cassalta, J. F. Marucco, P. Mendels, J. Arabski, and G. Collin, Physica C **171**, 419 (1990).

[4] H. Kageyama, K. Yoshimura, M. Kato, and K. Kosuge, J. Phys. Soc. Jpn. **64**, 2144 (1995).

[5] V. J. Emery, Phys. Rev. Lett. **58**, 2794 (1987).

[6] A. Aharony, R. J. Birgeneau, A. Coniglio, M. A. Kastner, and H. E. Stanley, Phys. Rev. Lett. **60**, 1330 (1988).

[7] R. J. Birgeneau, M. A. Kastner, and A. Aharony, Z. Phys. B **71**, 57 (1988); A. Aharony, R. J. Birgeneau, and M. A. Kastner, IBM J. Res. Dev. **33**, 287 (1989).

[8] R. E. Walstedt and W. W. Warren, Science **248**, 1082 (1990).

[9] H. Alloul, Physica B **169**, 51 (1991).

[10] A. Golnik, Acta Phys. Pol. A **84**, 165 (1993).
[11] M. Matsumura *et al.*, J. Phys. Soc. Jpn. **57**, 3297 (1988).
[12] P. Mendels, H. Alloul, J. F. Marucco, J. Arabski, and G. Collin, Physica C **171**, 429 (1990).
[13] A. Weidinger *et al.*, Phys. Rev. Lett. **62**, 102 (1989).
[14] R. F. Kiefl *et al.*, Phys. Rev. Lett. **63**, 2136 (1989).
[15] B. Keimer *et al.*, Phys. Rev. B **46**, 14 034 (1992).
[16] C. Goldenberg, M.S. thesis, Tel Aviv University, 1997.
[17] J. Villain, Z. Phys. B **33**, 31 (1979).
[18] J. Vannimenus, S. Kirkpatrick, F. D. M. Haldane, and C. Jayaprakash, Phys. Rev. B **39**, 4634 (1989).
[19] G. N. Parker and W. M. Saslow, Phys. Rev. B **38**, 11 718 (1988).
[20] L. I. Glazman and A. S. Ioselevich, Z. Phys. B **80**, 133 (1990).
[21] We tested Eq. (3) numerically, using the technique described in this paper, and found that it is quite accurate even for $r \sim 1$ (Ref. 16). We also examined the lattice size dependence of $|\boldsymbol{\mu}|$ and found that it is described quite well by considering the 2D electrostatic problem of a dipole at the origin, with zero potential on a circle with a radius of order $L/2$ around it (Ref. 16).
[22] A theoretical expression for the dependence of $|\boldsymbol{\mu}|$ on λ has been derived by A. S. Kovalev and M. M. Bogdan, Fiz. Tverd. Tela. **35**, 1773 (1993) [Phys. Solid State **35**, 886 (1993)]. They assumed that Eq. (3) holds for the spin *angles* with respect to the y axis instead of for their x component, S_x, and for all the spins. We calculated this dependence numerically, and our results disagree with their expression (Ref. 16). However, we were able to obtain a better description of this dependence by assuming that Eq. (3) holds as written, but only for spins at large enough distance from the AF bond (Ref. 16). We then minimize the Hamiltonian [Eq. (1)], solving (numerically) for the spins near the origin [for which we do not assume that Eq. (3) holds], and for $|\boldsymbol{\mu}|$. In this way, as we solve explicitly for more spins, we obtain a dependence of $|\boldsymbol{\mu}|$ on λ which is closer to our numerical results. However, we found that when using only a few spins, the solution oscillates nonmonotonically around our numerical results as we increase their number.
[23] We tested Eq. (4) for the case of two AF bonds numerically, and found surprisingly that it holds very well even for r as small as one lattice constant (Ref. 16).
[24] P. Gawiec and D. R. Grempel, Phys. Rev. B **44**, 2613 (1991).
[25] L. R. Walker and R. E. Walstedt, Phys. Rev. B **22**, 3816 (1980).
[26] C. M. Soukoulis, G. S. Grest, and K. Levin, Phys. Rev. B **28**, 1510 (1983).
[27] F. Mila and T. M. Rice, Physica C **157**, 561 (1989).
[28] T. Imai, J. Phys. Soc. Jpn. **59**, 2508 (1990).
[29] J. Rossat-Mignod, L. P. Regnault, M. J. Jurgens, C. Vettier, P. Burlet, J. Y. Henry, and G. Lapertot, Physica B **163**, 4 (1990).
[30] H. Kageyama, K. Yoshimura, M. Kato, and K. Kosuge, J. Phys. Soc. Jpn. **64**, 2144 (1995).
[31] J. B. Torrance, Y. Tokura, A. I. Nazzal, A. Bezinge, T. C. Huang, and S. S. P. Parkin, Phys. Rev. Lett. **61**, 1127 (1988).
[32] Y. Tokura, J. B. Torrance, T. C. Huang, and A. I. Nazzal, Phys. Rev. B **38**, 7156 (1988).
[33] J. L. Tallon, C. Bernhard, H. Shaked, R. L. Hitterman, and J. D. Jorgensen, Phys. Rev. B **51**, 12 911 (1995).
[34] N. Nucker *et al.*, Phys. Rev. B **51**, 8529 (1995).
[35] R. P. Gupta and M. Gupta, Phys. Rev. B **51**, 11 760 (1995).
[36] M. Muroi and R. Street, Physica C **246**, 357 (1995).
[37] A. Latge, E. V. Anda, and J. L. Morán-López, Phys. Rev. B **42**, 4288 (1990).
[38] G. Uimin and J. Rossat-Mignod, Physica C **199**, 251 (1992).
[39] B. W. Veal and A. P. Paulikas, Physica C **184**, 321 (1991).
[40] C. Y. Chen, E. C. Branlund, C. Bae, K. Yang, M. A. Kastner, A. Cassanho, and R. J. Birgeneau, Phys. Rev. B **51**, 3671 (1995).
[41] C. Y. Chen, R. J. Birgeneau, M. A. Kastner, N. W. Preyer, and T. Thio, Phys. Rev. B **43**, 392 (1991).